RAPIDITY SCAN IN HEAVY-ION COLLISIONS AT $\sqrt{s_{NN}} = 72$ GeV USING A VISCOUS HYDRODYNAMIC+CASCADE MODEL

Iurii Karpenko

SUBATECH, IN2P3/CNRS, Université de Nantes, IMT Atlantique
4 rue Alfred Kastler, 44307 Nantes cedex 3, France

(Received July 2, 2018; accepted December 31, 2018)

In this note, we discuss the rapidity dependence of the initial and final conditions for hydrodynamic evolution as well as the resulting basic hadronic observables in heavy-ion collisions at $\sqrt{s_{NN}} = 72$ GeV in the framework of a viscous hydrodynamic+cascade model vHLLE+UrQMD. The resulting rapidity dependences are driven to a big extent by the initial state, which is simulated with the UrQMD cascade. The results can serve as a prediction for future experiments such as the AFTER@LHC or the BES-II program at STAR.

DOI:10.5506/APhysPolB.50.141

1. Introduction

Heavy-ion collisions at the energies corresponding to the upper part of the RHIC Beam Energy Scan program represent an interesting case for exploration in the framework of hydrodynamic approach. On the one hand, the distributions of produced hadrons are approximately boost invariant in the range of a few units of rapidity around midrapidity — the picture well-established in heavy-ion collisions at the higher collision energies (top RHIC and LHC). On the other hand, at such energies, the effects of finite baryon density start to play a role due to finite baryon stopping.

In this respect, the AFTER@LHC program [1–4] looks promising, as it plans to use the LHC beam in a fixed target mode operation, colliding heavy ions (lead–lead, lead–xenon) at $\sqrt{s_{NN}} = 72$ GeV. Because of the fixed-target nature of the experiment, one can measure hadron production in a wide interval of rapidities, up to the projectile/target rapidity. Besides, the STAR experiment at RHIC plans Phase II of the Beam Energy Scan program with the upgraded detector which will allow for a larger rapidity coverage. In this work, we assess a rapidity dependence of the properties of matter created in such reactions, in the framework of viscous hydrodynamic+cascade model,

vHLLE+UrQMD. The structure is as follows: in Section 2, we briefly describe the model and show the rapidity dependence of thermodynamic parameters at the end of the hydrodynamic stage; in Section 3, we discuss the resulting observables, and make conclusions in Section 4.

2. Model and thermodynamics at particlization

We use a hydrodynamic+cascade model vHLLE+UrQMD to simulate the heavy-ion reactions at $\sqrt{s_{NN}} = 72$ GeV. The model is thoroughly described in [5], whereas here we highlight its main details. The initial stage of the reaction is described with hadron/string cascade UrQMD [6]. At the hypersurface of constant Bjorken proper time $\tau_0 = \sqrt{t^2 - z^2} = 0.64$ fm/c, the system is *fluidized*, *i.e.* the energy-momenta and charges of initial-state particles are distributed to the hydrodynamic grid. As the UrQMD cascade runs in Cartesian coordinate system which is different from Milne (τ–η) coordinate system used at the hydrodynamic stage, a transition is performed as follows: a modification is done to the initial state UrQMD cascade which blocks all hadron interactions in the domain $\tau = \sqrt{t^2 - z^2} > \tau_0$. Such a modified cascade is run till large enough Cartesian time $t = 400$ fm/c, and the final-state hadrons are propagated back in time to the hypersurface $\tau = \tau_0$ along straight trajectories. This way we obtain a 3-dimensional initial state with nonzero baryon, electric charge and — in event-by-event calculation — strangeness densities, which are propagated in the hydrodynamic stage by solving the corresponding charge conservation equations. In Fig. 1, we show event-averaged initial energy and baryon densities in the center of the transverse plane, $x = y = 0$, as a function of the spacetime rapidity η. We note that the baryon density distribution from the UrQMD initial stage is different from the other dynamical initial-state model in [7]. However, in our case, the initial state has also certain longitudinal flow which is stronger than the boost-invariant one. This results in a stronger propagation of the baryon density to higher geometrical rapidities. The initial state also contains a finite angular momentum of the system, which is important for the description of global Λ polarization in heavy-ion collisions [8]. The subsequent evolution is treated in the framework of a 3-dimensional event-by-event viscous hydrodynamic approximation with vHLLE code [9].

When the energy density in the local rest frame of a fluid element reaches the value of $\epsilon_{\rm sw} = 0.5$ GeV/fm^3, and the equation of state of matter is well-described in terms of a non-interacting hadron resonance gas, a so-called particlization is performed, *i.e.* change from fluid medium to particle description. At this point, we use the Cooper–Frye prescription [10]. The post-hydrodynamic evolution — hadronic rescatterings and resonance decays — is performed again with the UrQMD cascade.

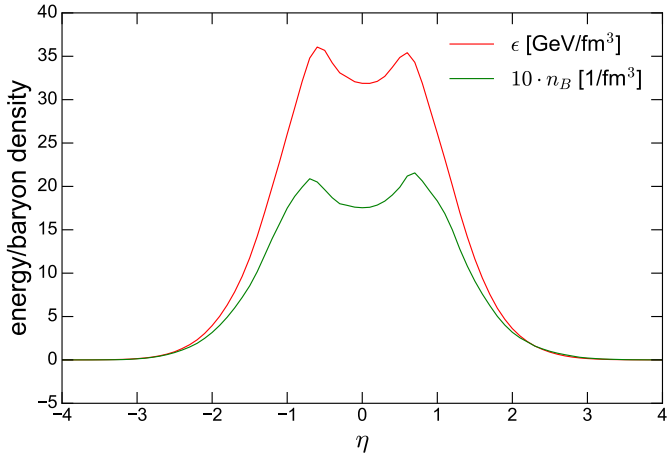

Fig. 1. Event-averaged initial energy and baryon densities for the hydrodynamic stage, in the center of the transverse plane, $x = y = 0$, as a function of the spacetime rapidity η. The simulation is performed for 0–5% central PbPb collision at $\sqrt{s_{NN}} = 72$ GeV.

The value of $\epsilon_{\rm sw} = 0.5$ GeV/fm^3 has been chosen in a previous analysis [5] to optimally describe the observables (including hadron chemistry) in the full range of RHIC BES energies, therefore, we use this setting as "universal" and use it to check what happens in a "rapidity scan" at a fixed collision energy instead of a collision beam energy scan.

Whereas the energy density at the particlization surface is fixed by construction, the charge densities (baryon, electric and strange) are given by the hydrodynamic evolution. As a result, the densities vary across the hypersurface. The Cooper–Frye prescription used to sample hadrons at the particlization hypersurface is based on grand canonical ensemble. Therefore, we recalculate temperature, baryon, electric and strange chemical potentials according to hadron gas EoS for given energy, baryon and strange densities on each element of particlization hypersurface. Naturally, the resulting temperature and chemical potentials vary across the hypersurface as well, which results in somewhat different chemical composition of hadrons depending on the positions of their production on the hypersurface. As this work focuses on the rapidity dependence, we amend the post-hydrodynamic part of the model in order to track the temperature and chemical potentials of the original surface element which produces each hadron. Then we visualize the distribution of temperatures and chemical potentials of the surface elements which produce hadrons of given momentum rapidity in Fig. 2. The color coding in this figure corresponds to intensity of particle emission at a given momentum rapidity from surface elements with a given temperature. The

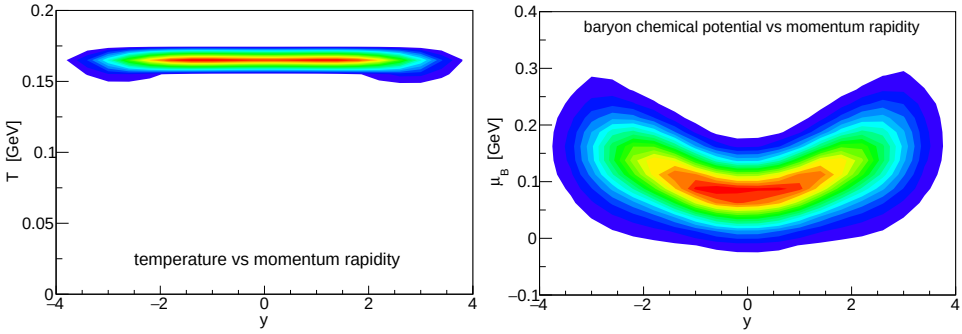

Fig. 2. Distribution of temperature and baryon chemical potentials across the particlization hypersurface as a function of momentum rapidity of produced hadrons. Color encodes the rate of particles produced with a given value of rapidity from a surface element with a given temperature or baryon chemical potential. The event-by-event hydrodynamic calculation is performed for 20–30% central PbPb collision at $\sqrt{s_{NN}} = 72$ GeV.

actual range of the temperatures and chemical potentials is even wider if one looks at all hypersurface elements irrespective of their contribution to the total particle production. Figure 2 demonstrates that *(i)* hadrons with higher momentum rapidities are, on average, produced from hydrodynamic medium with larger baryon chemical potential, *(ii)* even considering hadrons with fixed momentum rapidity, the variation of baryon chemical potential of the sources (surface elements) of their production is substantial. The latter constraints the conventional picture from studies in statistical hadronization model, which usually visualize particular collision energy probing a particular *point* on the QCD phase diagram via chemical freeze-out [11]. In fact, as one can see from Fig. 3, due to inhomogenity of the initial energy and baryon densities in all space directions, different fluid elements cover certain areas on the T–$\mu_{\rm B}$ plane in the course of their evolution. Fluid slices with higher spacetime rapidity cover strips at larger $\mu_{\rm B}$ as the initial ratio of baryon to energy density grows with (modulus of) rapidity. In this way, the different spacetime rapidity slices — which approximately correspond to momentum rapidity of the hadrons produced at particlization — scan different areas of the phase diagram in the course of their evolution. Whereas the trajectories in the T–$\mu_{\rm B}$ plane in Fig. 3 do not depend on the particlization criterion, the temperature and chemical potential distributions on the particlization hypersurface clearly do. However, the main factor here is independent propagation of baryon current in hydrodynamic phase. Therefore, a different choice of particlization criterion, *e.g.* a fixed temperature, will result in qualitatively similar distribution of baryon chemical potential at the particlization hypersurface.

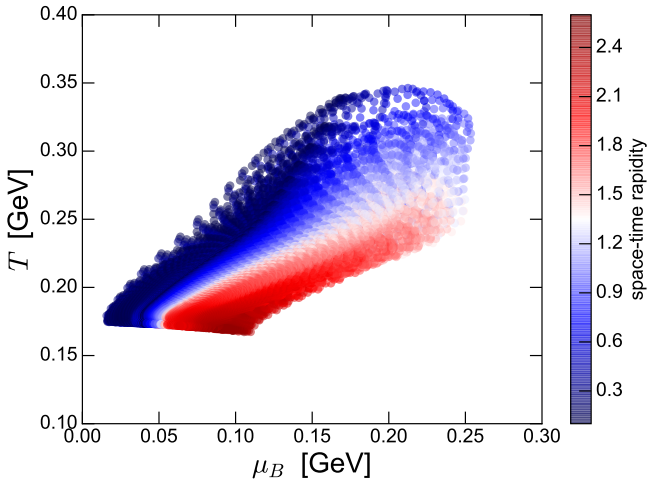

Fig. 3. Trajectories (represented by points) on the T–μ_{B} plane covered by the slices of the fluid corresponding to different rapidities. Color encodes the spacetime rapidity of the slice. The simulation is performed for the averaged initial state corresponding to 20–30% central Pb–Pb collisions at $\sqrt{s_{NN}} = 72$ GeV.

3. Rapidity dependence of observables

The resulting rapidity distributions of pions, kaons and protons in the model are shown in Fig. 4. As the temperature at the particlization hypersurface is virtually flat up to geometrical rapidity $\eta = \pm 3$, the rapidity shape of the pion and kaon yields is mostly defined by the change of the rapidity-differential effective volume $\Delta V_{\mathrm{eff}} = \int \mathrm{d}\sigma_\mu u^\mu$ with geometrical rapidity. In addition to that, the increase of mean baryon chemical potential away from midrapidity enhances the production of baryons and suppresses antibaryons. A shallow doubly-peaked structure in rapidity distribution for protons, combined with monotonic decrease of antiproton production with rapidity, results in somewhat more pronounced doubly-peaked structure for net protons, see the right panel of Fig. 4. However, comparing to existing results at $\sqrt{s_{NN}} = 62.4$ GeV from BRAHMS experiment at RHIC [12], one can observe that, whereas the overall trend in net proton rapidity distribution is qualitatively reproduced and its peak value is close to the experimental point, the hole at midrapidity is not wellreproduced due to the baryon charge distribution from UrQMD initial state. This can be attributed to a too strong baryon stopping in UrQMD model [13] and a larger baryon density in the central spacetime rapidity from the UrQMD initial state as a result.

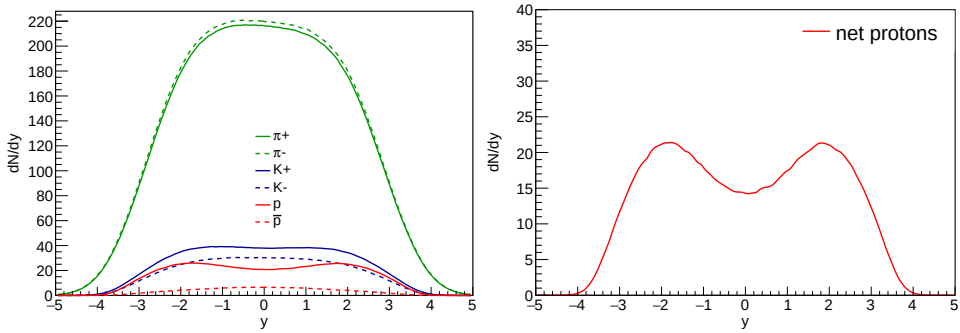

Fig. 4. Momentum rapidity distributions of identified hadrons (left panel) and rapidity distribution of net protons (right panel) at 0–5% central Pb–Pb collisions at $\sqrt{s_{NN}} = 72$ GeV from the event-by-event model calculations.

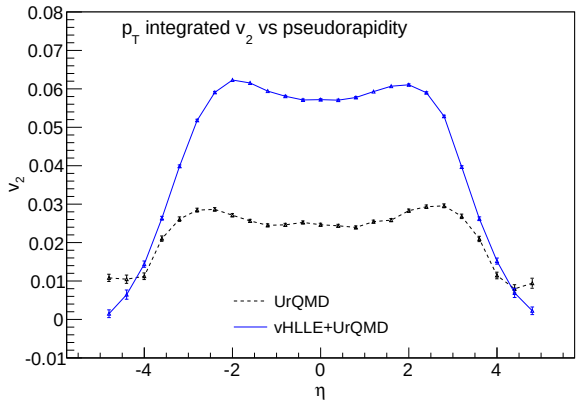

Fig. 5. Elliptic flow of all charged hadrons as a function of momentum rapidity, for 20–30% central Pb–Pb collisions at $\sqrt{s_{NN}} = 72$ GeV from the event-by-event model calculations.

Finally, we calculate the elliptic flow coefficient at different momentum rapidities using event plane method and show the results in Fig. 5. The elliptic flow exhibits peaks around pseudorapidity $\eta = \pm 2$. Such a rapidity structure is driven by two effects: *(i)* the eccentricity of the initial state slightly increases as one departs from zero spacetime rapidity region of the initial state, see Fig. 6, left, and *(ii)* because of the doubly-peaked structure of the initial energy density, the lifetime of the hydrodynamic stage as a function of geometrical rapidity peaks around $\eta = \pm 2$.

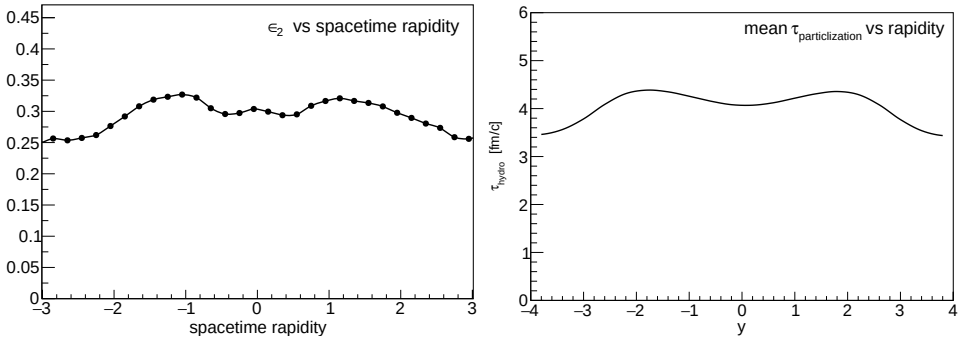

Fig. 6. Eccentricity of initial state as a function of spacetime rapidity (left panel) and mean proper time of particlization as a function of momentum rapidity of particle (right panel) for 20–30% central Pb–Pb collisions at $\sqrt{s_{NN}} = 72$ GeV from the event-by-event model calculations.

4. Conclusions

In this work, we have discussed the rapidity dependence of thermodynamic quantities and basic hadronic observables in $\sqrt{s_{NN}} = 72$ GeV PbPb collisions in the framework of viscous hydrodynamic+cascade model vHLLE+UrQMD. The initial state from the UrQMD cascade provides baryon, electric charge and strangeness densities along with the energy density. The initial baryon density profile is translated to the growth of effective baryon chemical potential with rapidity at the particlization (chemical freezeout) with no extra parameters.

More generally, different rapidity slices of the system cover different regions in the T–μ_B plane during their evolution. Such a "rapidity scan" in addition to the collision energy scan can be a finer tool to study the QCD phase diagram at the RHIC BES energies.

The author acknowledges enligthening discussions with Dr. Daniel Kikoła and Dr. Barbara Trzeciak. The work is supported by Region Pays de la Loire (France) under contract No. 2015-08473.

REFERENCES

[1] S.J. Brodsky, F. Fleuret, C. Hadjidakis, J.P. Lansberg, *Phys. Rep.* **522**, 239 (2013) [arXiv:1202.6585 [hep-ph]].

[2] B. Trzeciak *et al.*, *Few-Body Syst.* **58**, 148 (2017) [arXiv:1703.03726 [nucl-ex]].

[3] D. Kikoła *et al.*, *Few-Body Syst.* **58**, 139 (2017) [arXiv:1702.01546 [hep-ex]].

[4] L. Massacrier *et al.*, *EPJ Web Conf.* **171**, 10001 (2018) [arXiv:1712.01740 [hep-ex]].

[5] I.A. Karpenko, P. Huovinen, H. Petersen, M. Bleicher, *Phys. Rev. C* **91**, 064901 (2015) [arXiv:1502.01978 [nucl-th]].

[6] S.A. Bass *et al.*, *Prog. Part. Nucl. Phys.* **41**, 255 (1998); M. Bleicher *et al.*, *J. Phys. G* **25**, 1859 (1999).

[7] C. Shen, B. Schenke, *Phys. Rev. C* **97**, 024907 (2018) [arXiv:1710.00881 [nucl-th]].

[8] I. Karpenko, F. Becattini, *Eur. Phys. J. C* **77**, 213 (2017) [arXiv:1610.04717 [nucl-th]].

[9] I. Karpenko, P. Huovinen, M. Bleicher, *Comput. Phys. Commun.* **185**, 3016 (2014).

[10] F. Cooper, G. Frye, *Phys. Rev. D* **10**, 186 (1974).

[11] A. Andronic, P. Braun-Munzinger, K. Redlich, J. Stachel, *Nature* **561**, 321 (2018) [arXiv:1710.09425 [nucl-th]].

[12] I.C. Arsene *et al.* [BRAHMS Collaboration], *Phys. Lett. B* **677**, 267 (2009) [arXiv:0901.0872 [nucl-ex]].

[13] T. Anticic *et al.* [NA49 Collaboration], *Phys. Rev. C* **83**, 014901 (2011) [arXiv:1009.1747 [nucl-ex]].